Mitochondria-targeted cationic porphyrin-triphenylamine hybrids for enhanced two-photon photodynamic therapy

Fabien Hammerer, Florent Poyer, Laura Fourmois, Su Chen, Guillaume Garcia, Marie-Paule Teulade-Fichou, Philippe Maillard, Florence Mahuteau-Betzer

Mitochondria-targeted cationic porphyrin-triphenylamine hybrids for enhanced two-photon photodynamic therapy

Fabien Hammerer,[a,b,‡,†,*] Florent Poyer,[a,b,‡] Laura Fourmois,[a,b] Su Chen,[a,b] Guillaume Garcia,[a,b] Marie-Paule Teulade-Fichou,[a,b] Philippe Maillard,[a,b] Florence Mahuteau-Betzer[a,b,*]

a Institut Curie, Research Center, PSL Research University, Chemistry, Modelling and Imaging for Biology (CMIB) Bât 110-112, Centre Universitaire, F-91405 Orsay, France.

b CNRS UMR 9187 - INSERM U 1196, Paris-Saclay Université Paris Sud 11, Bât 110-112, Centre Universitaire, Rue Henri Becquerel F-91405 Orsay Cedex, France.

† Current address: Chemistry Department, McGill University, 801 Sherbrooke Street West, Montreal, QC, H3A 0B8, Canada.

‡ These authors contributed equally to this work.

KEYWORDS: two-photon absorption, photodynamic therapy, cancer, vinyltriphenylamine

ABSTRACT

The proof of concept for two-photon activated photodynamic therapy has already been achieved for cancer treatment but the efficiency of this approach still heavily relies on the availability of photosensitizers combining high two-photon absorption and biocompatibility. In this line we recently reported on a series of porphyrin-triphenylamine hybrids which exhibit high singlet oxygen production quantum yield as well as high two-photon absorption cross-sections but with a very poor cellular internalization. We present herein new photosensitizers of the same porphyrin-triphenylamine hybrid series but bearing cationic charges which led to strongly enhanced water solubility and thus cellular penetration. In addition the new compounds have been found localized in mitochondria that are preferential target organelles for photodynamic therapy. Altogether the strongly improved properties of the new series combined with their specific mitochondrial localization lead to a significantly enhanced two-photon activated photodynamic therapy efficiency.

INTRODUCTION

Among the emerging techniques for the treatment of cancer, Photodynamic Therapy (PDT) is considered one of the most promising and has gained significant momentum in clinics over the last decades (*1*-*3*). It relies on the sensitization of molecular oxygen to its singlet excited state by a photosensitizer (PS) excited at the appropriate wavelength.(*4*) Cytotoxic activity is due to ROS

formation and thus achieved only in the irradiated area and healthy tissues are spared, leading to minimal secondary effects for patients.(*5*) In this context, two-photon absorption (2PA) attracted the attention of the field.(*6-8*) Indeed, 2PA is typically achieved at the focal point (volume of around few femtoliters) of femtosecond pulsed lasers allowing a high spatial resolution. This phenomenon is due to the simultaneous absorption of both photons and necessitates a high photonic density.(*9*) Furthermore the wavelengths in use for 2PA are situated in the near infrared and correspond to the physiological optical window where light penetration can reach the centimeter scale. (*10*) Since the demonstration in 2008 that two-photon activated PDT (2PA-PDT) could be applied to whole tumors,(*6, 11*) a lot of efforts have been put into the development of 2PA-PS.(*12*) Their design remains however delicate since the large π-conjugated systems required for 2PA are also highly hydrophobic and usually incompatible with biological media.

In an attempt to adapt this approach to 2PA-PDT, we recently reported the synthesis and properties of π-conjugated porphyrin-triphenylamine hybrids displaying high singlet oxygen production quantum yield and two-photon absorption.(*12*) The biological potential of this first generation of hybrids was however significantly limited by poor solubility in aqueous media. In the aim optimizing this feature we prepared a second generation of hybrids systematically methylated on the pyridine rings which afforded three cationic hybrids bearing two or four charges respectively (Figure 1). The biscationic compounds are functionalized by triethylene glycol (**P_{TEG}TP)** or α-mannosyl groups **(P_{Man}TP)** in para-position of meso-phenyl moieties. The glycosylation of the porphyrin is devoted to specific targeting of retinoblastoma cells that overexpress mannose and galactose-specific membrane lectins, as shown is previous work.(*13*) (*14*) The more conjugated tetracationic **$P_{TEG}(TP)_2$** containing two triphenylamine moieties was expected to exhibit a high hydrosolubility together with a red-shift in absorption and emission spectra.

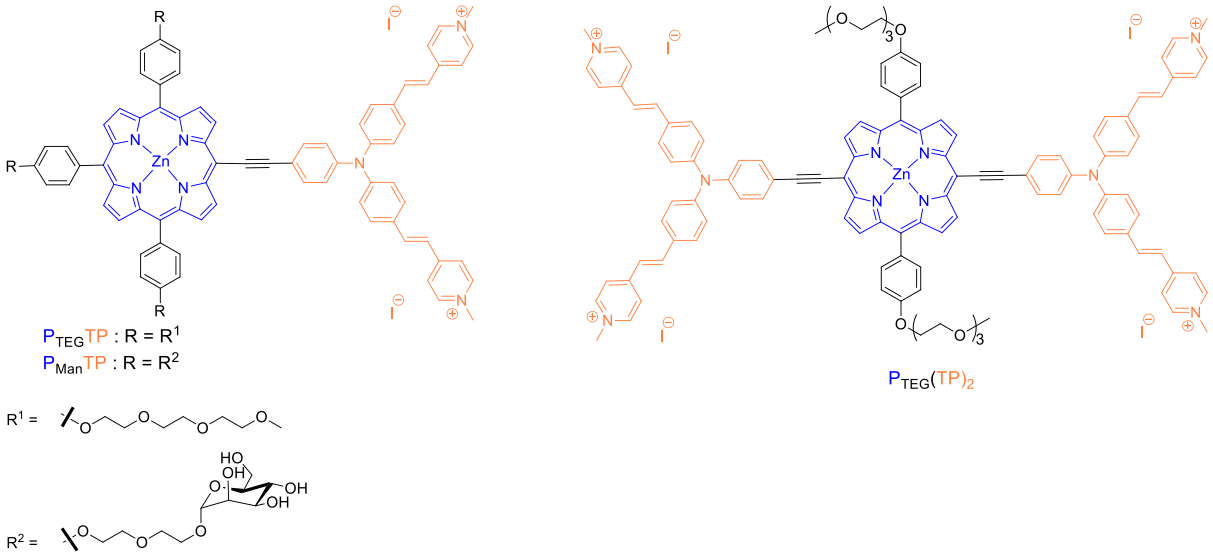

Figure 1: Structures of the cationic hybrids **P_{Man}TP**, **P_{TEG}TP** and **$P_{TEG}(TP)_2$**

While the main purpose of the methylation was to increase aqueous solubility, several other considerations interested us. Firstly, the vinyl pyridinium triphenylamine (TP) motif was identified by our team as a strong DNA minor groove binder.(*15*) While it is poorly emissive in aqueous solution due to fast non-radiative deexcitation, fluorescence emission increases dramatically upon DNA binding. Secondly, we previously showed that although TP stain nuclear DNA in fixed cells, similarly to DAPI, these compounds are preferentially localized in mitochondria in live cells.(*16*) Therefore the newly prepared methylated hybrids **P_{TEG}TP**, **P_{Man}TP** and **$P_{TEG}(TP)_2$** were anticipated to localize in mitochondria, that represents a preferential target organelle for PDT.(*7, 17, 18*) Indeed, mitochondria are known to be highly sensitive to oxidative stress and their disruption leads to apoptosis.(*19*)

This study presents the synthesis of methylated hybrids along with their photophysical properties. These compounds were also evaluated for their cellular phototoxicity versus dark toxicity, their localizations were determined by one photon (1PA) and 2PA confocal microscopy on two different cancer cell lines (retinoblastoma Y79 and colon adenocarcinoma HT-29 cells). The 2PA confocal microscopy enabled us to determine the 2PA phototoxicity.

Results and discussion

Synthesis

P_{TEG}TP and **P_{Man}TP** were obtained by methylation of their neutral precursors **1a** and **1b** (prepared as previously described) with a large excess of methyl iodide in quantitative yield (scheme 1).

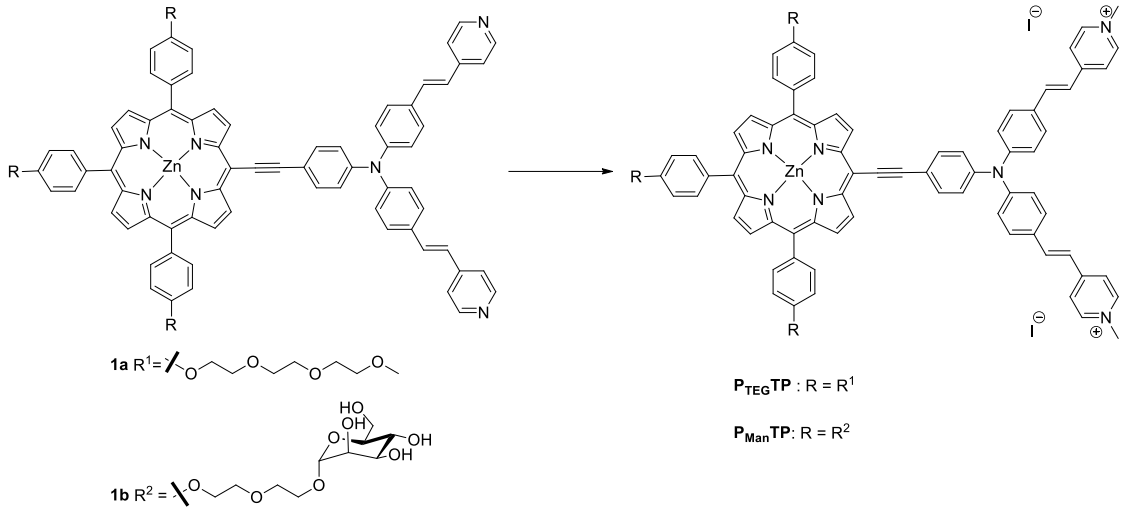

Scheme 1: Synthesis of $\mathbf{P_{TEG}TP}$, $\mathbf{P_{Man}TP}$.Conditions: MeI, DMF, r.t.

The neutral precursors of $\mathbf{P_{TEG}(TP)_2}$ were prepared by a synthetic pathway inspired by the one used for the preparation of **1a** and **1b** (Scheme 2). Bromination of derivative **2** by *N*-bromosuccinimide afforded the dibromo zinc complex **3** in a good yield. Sonogashira cross-coupling reaction with excess of trimethylsilylacetylene (TMSA) afforded compound **4** in 84% yield. Compound **5** was synthesized in two steps in 46% yield from **4**: first TMS groups were removed with *n*-tetrabutylammonium fluoride (TBAF), then a double Heck coupling reaction with 4,4'-diformyl-4''-iodotriphenylamine was performed. Compound **6** was obtained in 58% yield by a Horner-Wadsworth-Emmons reaction with diethyl[(pyridine-4-yl)methyl]phosphonate. All final compounds were isolated in their E configuration as observed by ^{1}H NMR ($^3J_{H-H'} \approx 16$ Hz).

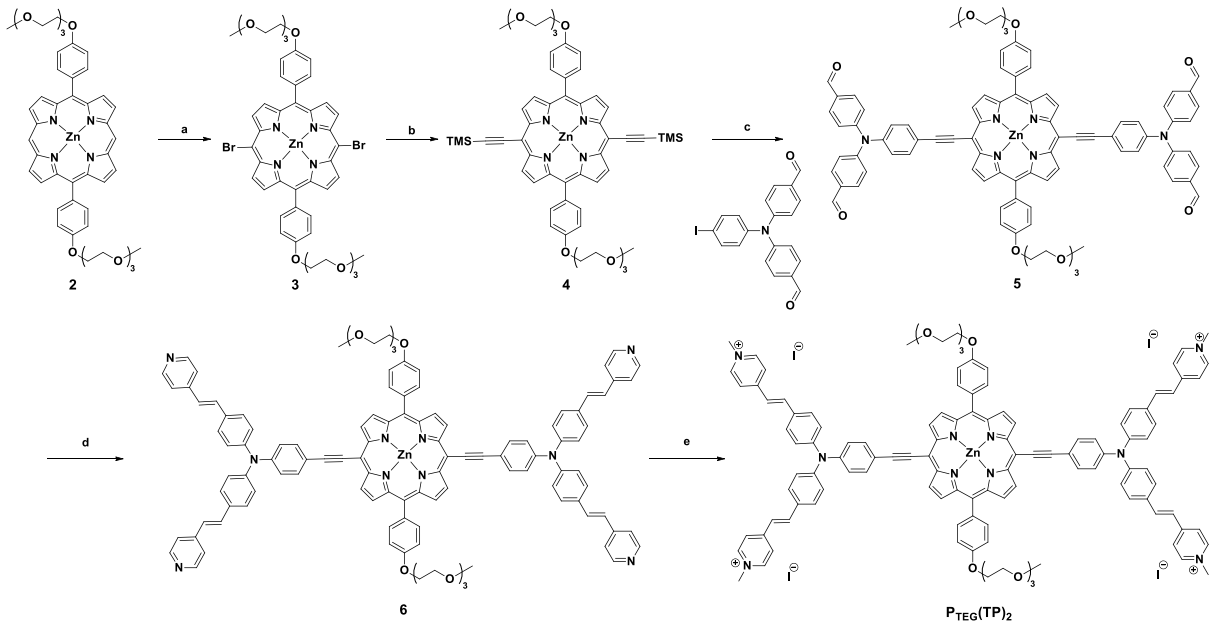

Scheme 2: Synthesis of compound $\mathbf{P_{TEG}(TP)_2}$. a) NBS, $CHCl_3$, pyridine, 0 °C to r.t., 30 min, 93 %; b) TMSA, $Pd(PPh_3)_2Cl_2$, CuI, THF, Et_3N, -180 °C to r.t., 16 h, 84 %; c) 1- TBAF, THF, DCM,r.t., 30 min, 2- Pd_2dba_3, $AsPh_3$, THF, Et_3N, r.t., 20 h, 46 % over two step; d) $PyrCH_2PO(OEt)_2$, NaH, THF, r.t., 24 h, 58 %; e) MeI, DMF, r.t., 18 h, 94%.

Photophysical properties

The UV absorption spectra of compounds $\mathbf{P_{TEG}TP}$, $\mathbf{P_{Man}TP}$ and $\mathbf{P_{TEG}(TP)_2}$ were recorded in water and are presented in Figure 2A. The absorption profiles obtained are typical of conjugated porphyrins with a red-shifted Soret band at 450 nm for $\mathbf{P_{TEG}TP}$ and $\mathbf{P_{Man}TP}$, at 470 nm for $\mathbf{P_{TEG}(TP)_2}$ as well as intense and shifted Q bands between 570 and 720 nm. In the case of $\mathbf{P_{TEG}(TP)_2}$, only one Q band can be observed (Table 1). The fluorescence emission spectra of the methylated hybrids were recorded in water (Figure 2B) and display typical albeit red-shifted porphyrinic profiles with maxima around 650 nm for $\mathbf{P_{TEG}TP}$ and $\mathbf{P_{Man}TP}$ and 715 nm for $\mathbf{P_{TEG}(TP)_2}$ with a weak band on the low energy side.

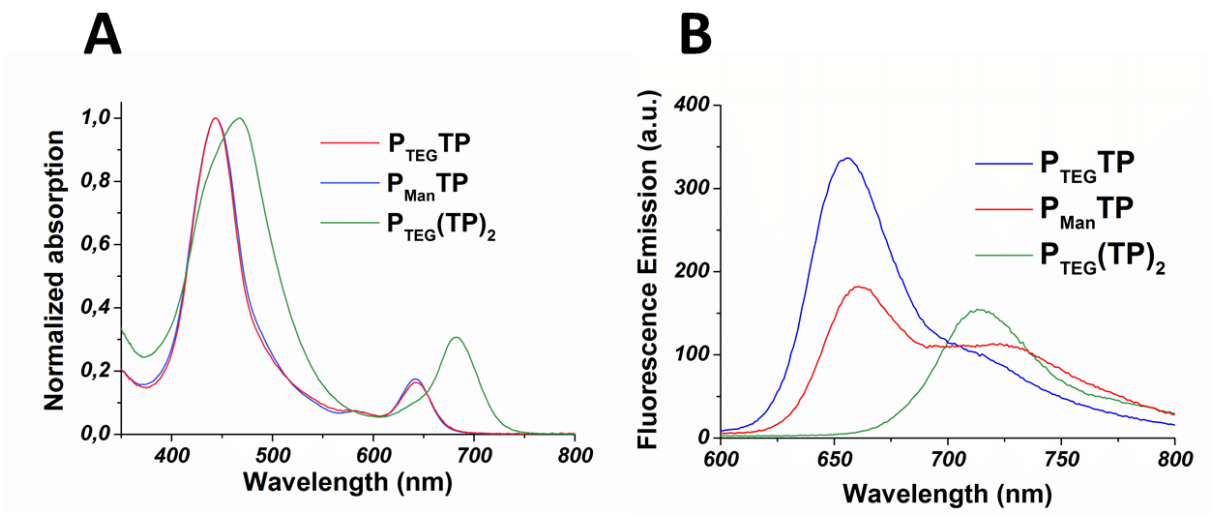

Figure 2: A) Normalized absorption spectra of $\mathbf{P_{TEG}TP}$, $\mathbf{P_{Man}TP}$ and $\mathbf{P_{TEG}(TP)_2}$ in water; B) Fluorescence emission spectra of the hybrids (1 µM) in water following excitation at the maximum of the Soret band.

	Soret Band		Q Bands			
Compound	λ_{max} (nm)	ε ($mM^{-1}.cm^{-1}$)	λ_{max} (nm)	ε ($mM^{-1}.cm^{-1}$)	λ_{max} (nm)	ε ($mM^{-1}.cm^{-1}$)
$\mathbf{P_{TEG}TP}$	444	183.6	581	13.8	642	34.0
$\mathbf{P_{Man}TP}$	443	65.9	577	5.0	643	11.0
$\mathbf{P_{TEG}(TP)_2}$	467	114.3	absent	absent	682	34.7

Table 1: Absorption maxima and molar absorption coefficients of compounds **P_{TEG}TP, P_{Man}TP** and **$P_{TEG}(TP)_2$** in water.

A solvatochromism study on **P_{TEG}TP** was conducted (see ESI S.3) and revealed a slight bathochromic shift of both the Soret and Q_I bands when increasing the solvent polarity revealing the internal charge transfer (ICT), a characteristic of these transitions and delocalization of electrons along the ethynyl bridge between the porphyrin and the TP core. ICT character is stronger for the Q band which has been reported as especially sensitive to electron delocalization. In order to further probe the electronic levels at the origin of fluorescence emission, we looked at the excitation spectra of the compounds. The spectra presented in Figure 3 are normalized in order to superimpose the Q_I bands of the excitation and the absorption spectra. They show an important difference between absorption and fluorescence excitation in the Soret area which indicates an important energy loss along the transition from S_2 to S_1 and confirms the existence of an energy dissipating mechanism, which is especially efficient for **$P_{TEG}(TP)_2$**. Such a phenomenon should also lead to the excitation wavelength dependence of the fluorescence quantum yields, but this hypothesis could not be verified due to the low fluorescence emission of the compounds.

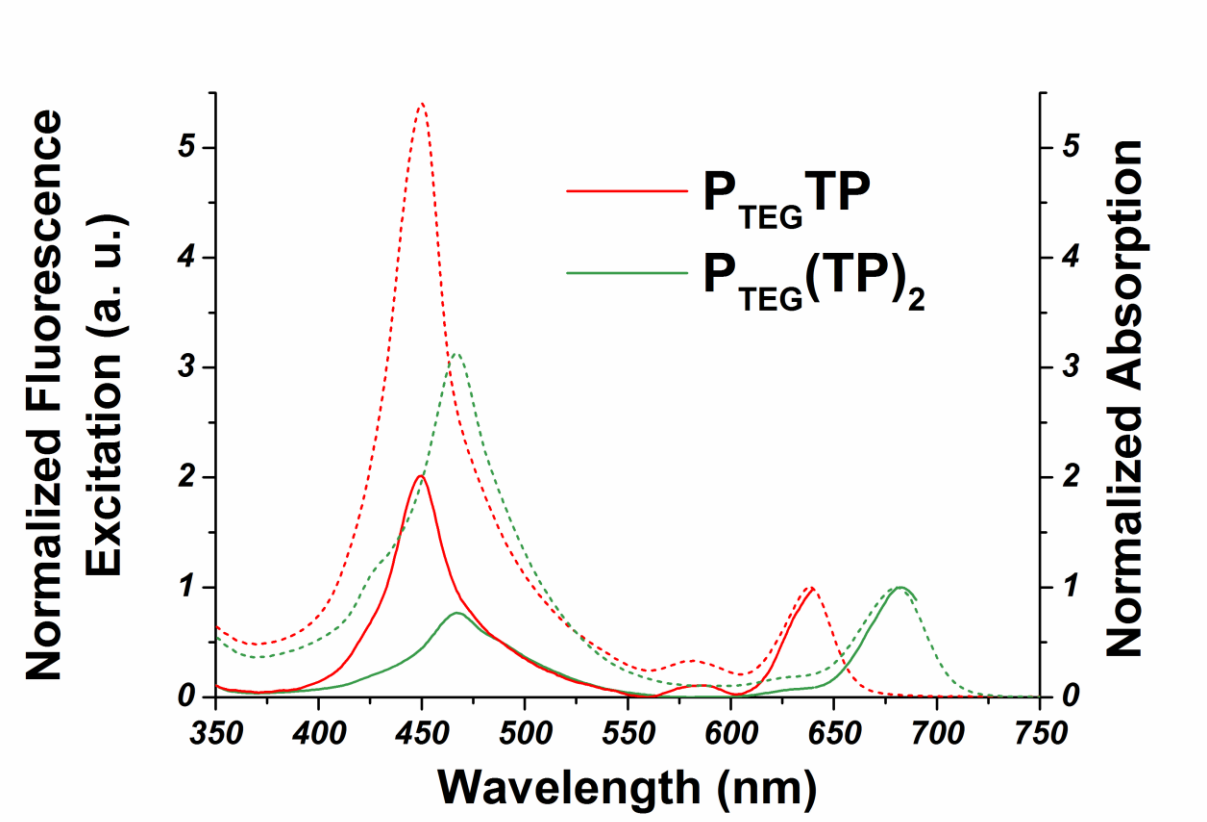

Figure 3: Normalized fluorescence excitation (continuous line) and UV absorption (dotted line)

spectra of the hybrids in DMF. The fluorescence was monitored at the emission maximum of the compounds.

The fluorescence quantum yields of cationic derivatives in DMF excited in the Soret band are extremely low (<0.1%) and are given as an indication, although the fluorescence quantum yields of their neutral analogs were around 2-3% (table 2). This 10-fold decrease compared with their neutral precursors confirms the existence of the anticipated non-radiative deexcitation pathway linked to the methylation of the pyridine rings.

Previous work by our team has shown that the spectroscopic properties of pyridinium-conjugated triphenylamines were significantly modified by solvent viscosity. In particular, dissolution in glycerol leads to higher absorption (one and two-photon) and fluorescence emission. Hence we recorded the absorption spectra of the hybrids in glycerol (Figure S3). A strong increase of the absorption at 500 nm is observed for all compounds leading to an almost symmetric Soret band for $\mathbf{P_{TEG}(TP)_2}$ following the stabilization of the cationic branches of the TP part by the viscous solvent. On the other hand, no noteworthy modification is observed in the Q band area. These modifications were accompanied by a strong fluorescence emission increase for all compounds, allowing the measurement of the emission quantum yields (Table 2).

Both the strong enhancement and porphyrin profile of the fluorescence emission of the hybrids suggest the existence of an energy transfer process from the TP towards the porphyrin in glycerol. Despite attempts to confirm this hypothesis through fluorescence lifetime studies, the strong overlap of the absorption bands prevented any definite conclusion. Due to the extremely low fluorescence of the compounds, our attempts to determine the compounds cross section using two-photon excitation fluorescence method also remained unsuccessful.

Compound	Φ_f[b]	Φ_Δ[b]	Φ_f[c]
1a	0.03[a]	0.74[a]	nd
$\mathbf{P_{TEG}TP}$	< 0.001	0.04	0.04
1b	0.02[a]	0.84[a]	nd
$\mathbf{P_{Man}TP}$	< 0.001	0.08	0.09
6	0.03	0.65	nd

$\mathbf{P_{TEG}(TP)_2}$	< 0.001	0.14	0.09

[a] as published in ref, [b] measured in freshly distilled DMF, [c] measured in glycerol, nd non determined

Table 2: Fluorescence (Φ_f) and singlet oxygen production quantum yields (Φ_Δ) of cationic hybrids and their neutral counterparts (excitation at the maximum of the Soret band).

One-photon singlet oxygen generation

The photosensitizing capacities of the hybrids were evaluated by measuring the singlet oxygen production quantum yield *via* the singlet oxygen luminescence method in DMF. The results are presented in Table 2 and show a decrease by a factor of 18 for **P_{TEG}TP** and 10 for **P_{Man}TP** and nearly 5 for **$P_{TEG}(TP)_2$** compared to their respective non-methylated analogs. These results were confirmed by a qualitative study using DPBF degradation by singlet oxygen in a home-made test (Figure S4). This is another confirmation for the energy dissipating mechanism.

Interaction with DNA

We investigated the affinity of the hybrids for a duplex DNA oligonucleotide, DrewAT (autocomplementary sequence: CGCGAAATTTCGCG) structured as a double helix. While the absorption spectra of **P_{TEG}TP**, **P_{Man}TP** and **$P_{TEG}(TP)_2$** were only marginally modified by the addition of DNA (Figure S5), a strong broad fluorescence emission band appeared between 500 and 750 nm which was attributed to TP emission (Figure 4A for **P_{TEG}TP** and **$P_{TEG}(TP)_2$**). The similarity with previously studied triphenylamines points to a minor groove binding interaction.

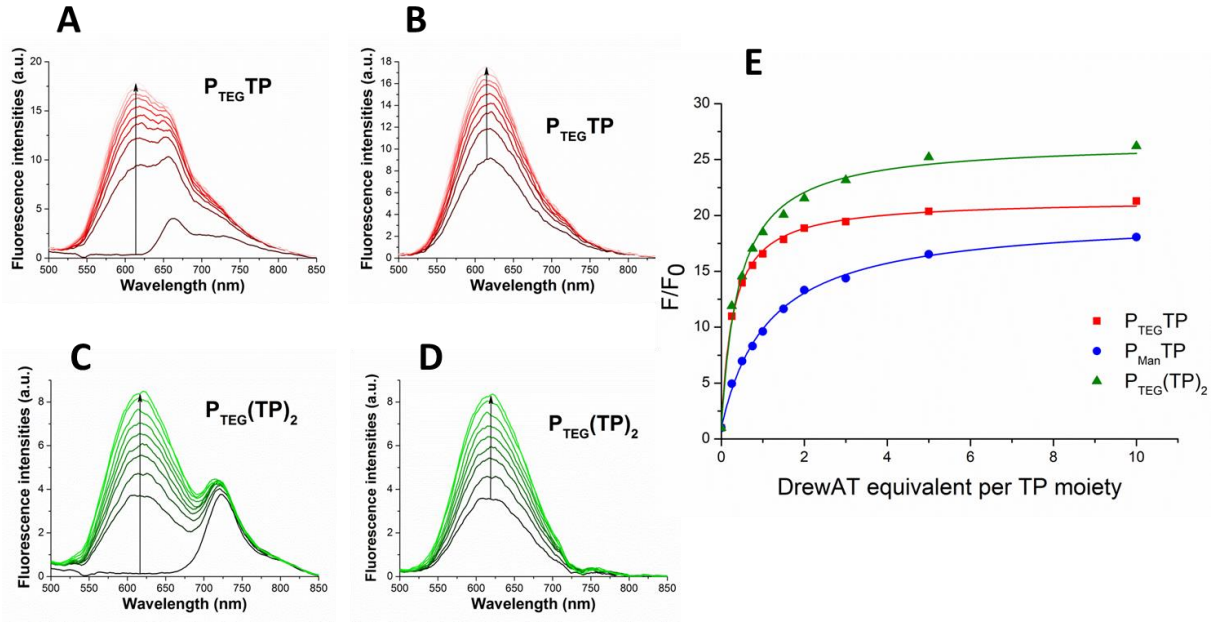

Figure 4: Fluorescence emission of A) **P_{TEG}TP** and C) **$P_{TEG}(TP)_2$** upon DrewAT titration (1 µM, exc.: 450 nm, 0 to 10 eq./TP moiety), in a buffer solution sodium cacodylate 10 mM, NaCl 100 mM. Fluorescence of B) **P_{TEG}TP** and D) **$P_{TEG}(TP)_2$** without initial porphyrin contribution. E) Fluorescence enhancement of compounds **P_{TEG}TP**, **P_{Man}TP** and **$P_{TEG}(TP)_2$** as a function of DrewAT equivalents by addition of DNA, between 500 and 620 nm for hybrids **P_{TEG}TP** and **P_{Man}TP** between 500 and 650 nm for **$P_{TEG}(TP)_2$**.

Fluorescence enhancement F/F_0 was plotted as a function of DNA equivalents reported to the number of TP moieties on the hybrid (Figure 4E) where F is the integrated fluorescence for the half band between 500 and 620 nm to remove porphyrin contribution. F_0 is the integrated fluorescence before DNA addition. All hybrids displayed a fluorescence increase of at least 17-fold with the best affinity for **P_{TEG}TP**. The titration curves were fitted on a mathematic model in order to evaluate the affinity of the hybrids towards DNA. The same affinity for DNA is observed for **P_{TEG}TP** and **$P_{TEG}(TP)_2$** (K_A~$3x10^6$ M^{-1}). This indicates that the two TP moieties of **$P_{TEG}(TP)_2$** interact with DNA independently**.** A slightly lower affinity of **P_{Man}TP** for DNA was determined; it can be attributed to the glycosyl groups steric hindrance (K_A~$8x10^5$ M^{-1}).

To determine if any energy transfer occurred, the free hybrid emission was subtracted from all spectra which led to a symmetrical band (Figure 4C and D) suggesting a constant participation of this part of the hybrid and the absence of energy transfer one way or another upon DNA binding. This result was confirmed by the constant singlet oxygen production in the presence or absence of DNA duplex (data not shown). Furthermore, the presence of DNA did not affect the emission of the porphyrin part following excitation in the Q band (633 nm) as illustrated in the Figure S6 as could be expected considering the levels of the orbitals.

This difference in behavior compared to glycerol reveals the existence of an alternate deexcitation pathway upon DNA binding in which the TP→Porphyrin energy transfer is prevented. The rigidity of the alkyne linker is probably at the origin of this singular behavior since efficient FRET was observed for a similar flexible porphyrin-vinylpyridinium carbazole compound.(*20*)

Cellular localization

Confocal fluorescence microscopy experiments were performed to investigate the cellular localization of the compounds **P_{TEG}TP**, **P_{Man}TP** and **$P_{TEG}(TP)_2$**. They were carried out on HT-29 (colorectal adenocarcinoma) and Y79 (retinoblastoma) cell lines with fixed and living cells. According to the absorption and emission spectra of the compounds, images were acquired using two excitation

wavelengths (458 nm and 633 nm) corresponding to either conjoined excitation in the Soret and TP bands or selective excitation in the porphyrin Q bands respectively.

Observation of fixed HT-29 cells after 24 hours incubation with compound **P_{TEG}TP** reveals a dual localization of the hybrid. Emission signals were harvested as illustrated in Figure 5A for **P_{TEG}TP**. The first signal (520-620 nm, Figure 5B, green) corresponds to the emission of the DNA-bound hybrid following excitation in the Soret area (458 nm). This behavior is in accordance with previous results obtained with TP compounds which are known to stain the nucleus in fixed cells. Meanwhile, emission of unbound hybrid is observed between 620 and 800 nm (Figure 5C, red) at the vicinity of the cell membrane where it seems to aggregate. Weak signals are also detected in the nuclei due to the superimposition with the DNA-bound species at these wavelengths. In order to avoid this weak signal, the excitation in the Q band area (633 nm) was chosen and led only to DNA-unbound hybrid emission (Figure 5D, blue). Overlays of the signals were produced without (Figure 5E) and with brightfield (Figure 5F) using the corresponding colors. As expected, the free hybrid appeared in magenta (merge of red and blue) on the overlays (Figures 5E and 5F) and the DNA-bound species in bright green, thereby revealing complete separation of the two signals. Hybrids **P_{Man}TP** and **$P_{TEG}(TP)_2$** exhibited similar behaviors (Figures S8 and S9) thereby confirming the hybrids affinity for DNA but also their tendency to aggregate in culture medium.

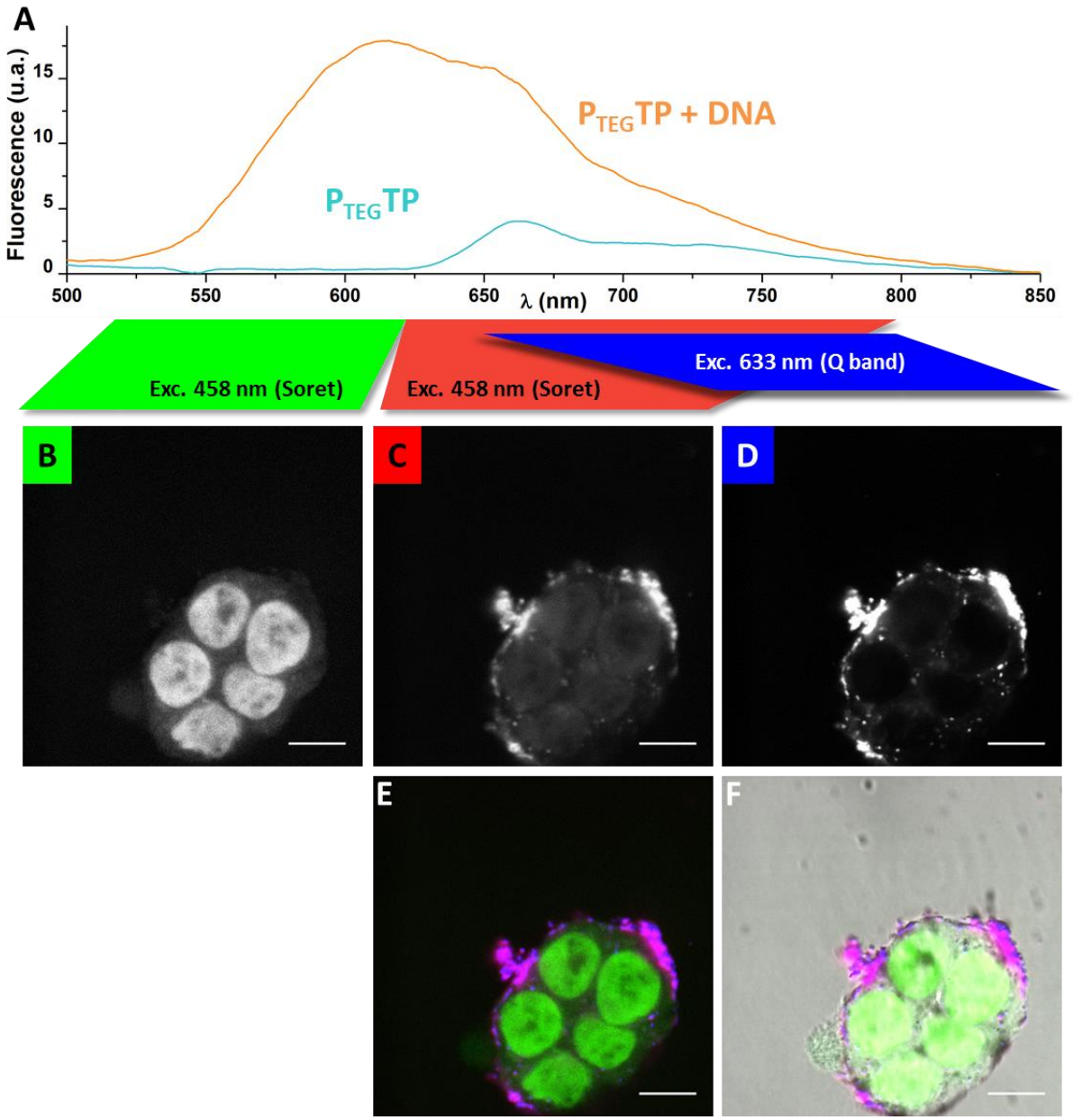

Figure 5: Fluorescence imaging of immobilized HT-29 cells with compound **P_{TEG}TP**. A) Emission spectra of **P_{TEG}TP** (blue) and **P_{TEG}TP** bound to DNA (green) after excitation at 450 nm; B) Emission signal between 520 and 620 nm following excitation in the Soret band (458 nm); C) Emission signal between 621 and 800 nm following excitation in the Soret band (458 nm); D) Emission signal between 643 and 800 nm following excitation in the Q band (633 nm); E) Overlay of B, C and D; F) Overlay of E and brightfield image. Scale bar 10 µm.

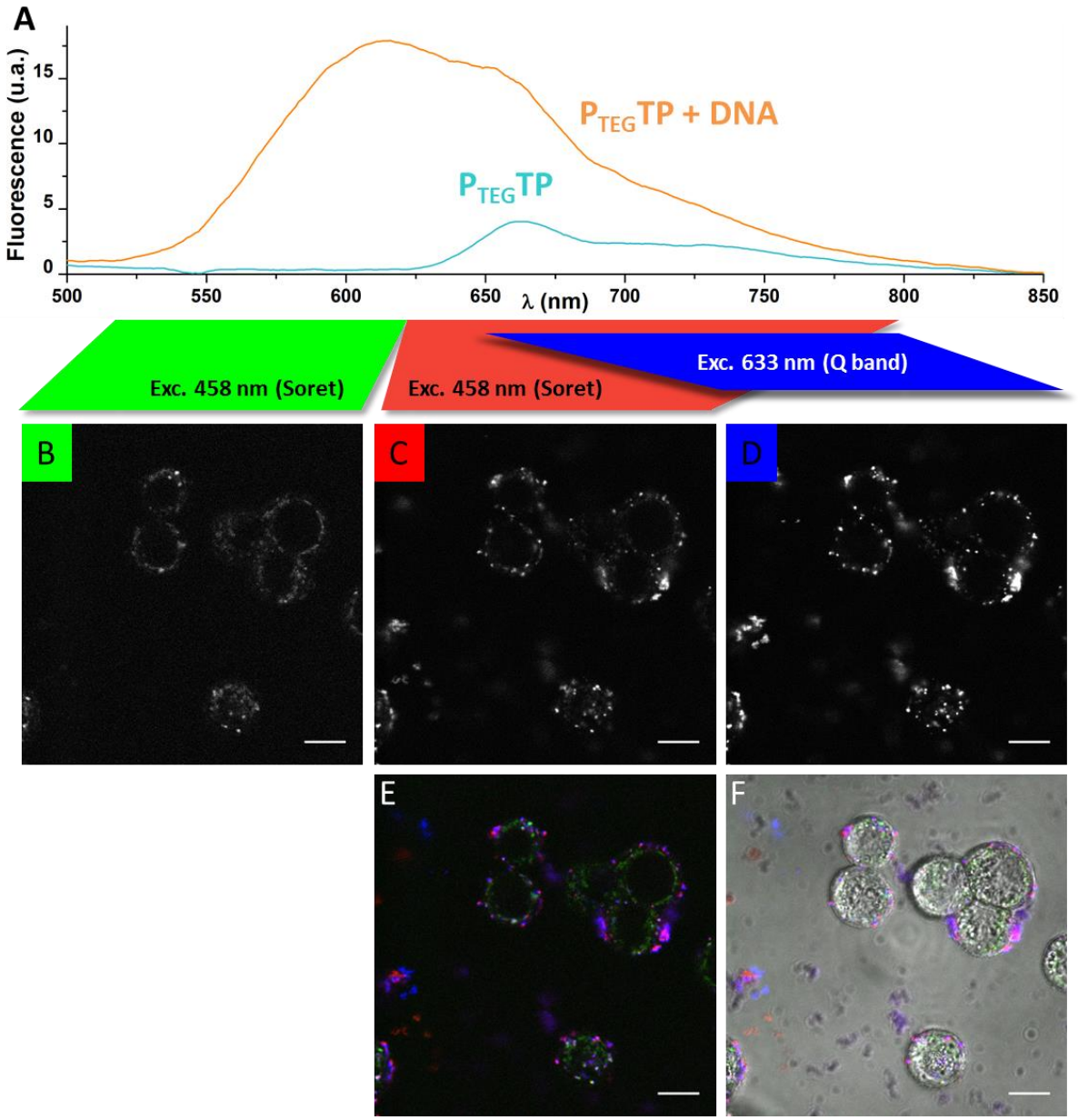

Figure 6: Fluorescence imaging of live HT-29 cells with compound **P_{TEG}TP**. A) Emission spectra of **P_{TEG}TP** (blue) and **P_{TEG}TP** bound to DNA (orange) after excitation at 450 nm. B) Emission signal between 520 and 620 nm following excitation in the Soret band (458 nm). C) Emission signal between 621 and 800 nm following excitation in the Soret band (458 nm). D) Emission signal between 643 and 800 nm following excitation in the Q band (633 nm). E) Overlay of B, C and D. F) Overlay of E and bright field image. Scale bar 10 µm.

The hybrids behaved in a significantly different manner in live HT-29 cells as illustrated in Figure 6 for **P_{TEG}TP** (Figure S10 and S11 for **P_{Man}TP** and **$P_{TEG}(TP)_2$** respectively). Strikingly, no emission from the nucleus could be observed following excitation at either 458 or 633 nm (Figure 6B-D). Instead, typical

DNA-bound fluorescence was detected in organelles located around the nucleus which are thought to be mitochondria (Figure 6B). Due to the wide absorption spectra of the compound, co-staining experiments with mitochondria trackers could not be realized. However, mitochondria are the only organelles containing DNA and therefore are more likely to induce TP emission. This result is fully consistent with our previous work that showed the preferential accumulation of cationic triphenylamine derivatives in mitochondria.(*16, 21*) Moreover, the hybrids are lipophilic cations and therefore are susceptible to be sequestrated in mitochondria due to the high negative membrane potential of this organelle. Free hybrid fluorescence emission (Figures 6C and 6D) is also observed at the cell membrane and in the cytosol probably due to their immobilization.

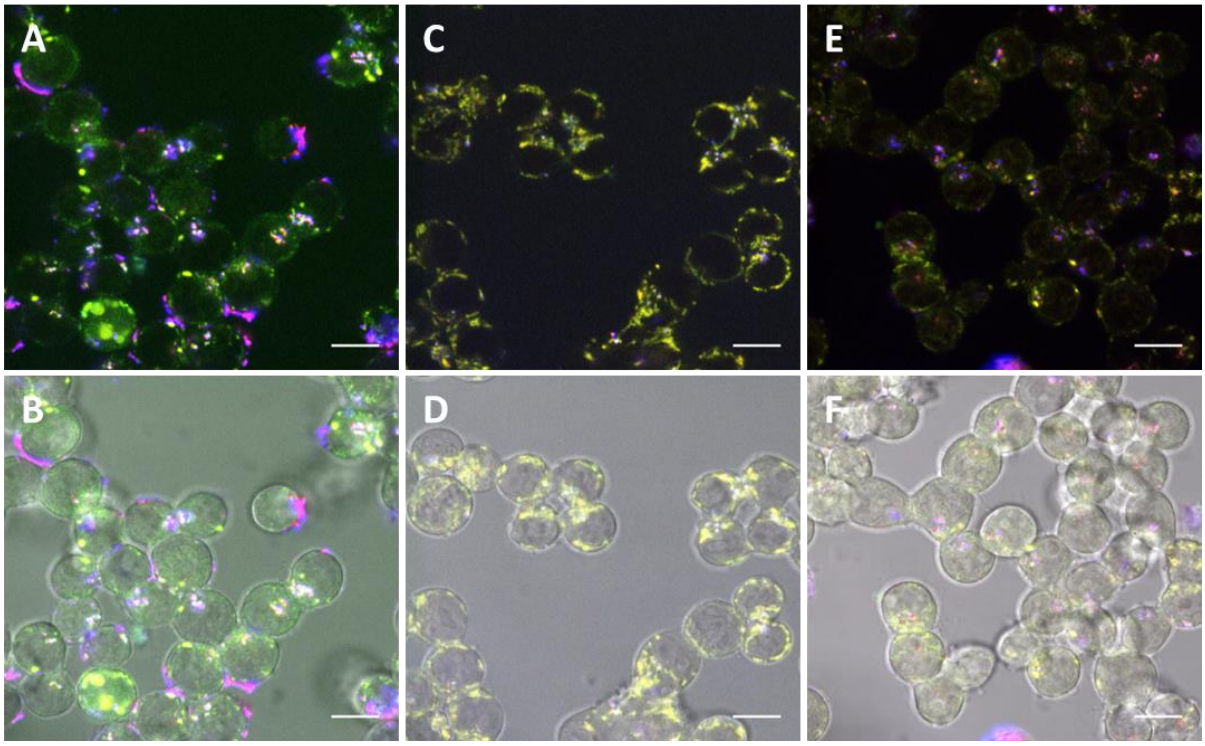

Figure 7: Fluorescence imaging of live Y79 cells with compounds **P_{TEG}TP** (A and B), **P_{Man}TP** (C and D) and **$P_{TEG}(TP)_2$** (E and F). Top: Overlay of signals collected between 520-620 nm following excitation at 458 nm (green), 621-800 nm following excitation at 458 nm (red) and between 650-800 nm (or 650-725 nm only for **$P_{TEG}(TP)_2$**) following excitation at 633 nm (blue). Bottom: Overlay of the same signals with brightfield image. Scale bar 10 µm

The hybrids were then observed in live Y79 cells using the same excitation and emission wavelengths (Figure S12 to S14). **P_{TEG}TP** (Figures 7A and 7B) and **$P_{TEG}(TP)_2$** (Figures 7E and 7F) behaved in similar fashion as in live HT-29 cells. Conversely, the glycosylated compound **P_{Man}TP** showed superimposition of the signals red and green as materialized by the predominance of yellow on the overlay (Figure 7C

and 7D). This compound is localized in discrete organelles at the periphery of the large cell nuclei characteristic of the retinoblastoma cells and very few external aggregates were observed. As already observed above, the DNA-bound hybrid could also be detected between 620 and 800 nm after a 458 nm excitation (Figure S13C). For this compound which is more permeant due to enhanced solubility, only the DNA-bound hybrid was observed leading to the merge of the two signals in mitochondria, corresponding to the colocalization of DNA-bound and free hybrids in the matrix of mitochondria.

Overall, the cationic hybrids display highly enhanced internalization capacity compared to their neutral counterparts and allowed confocal microscopy experiments despite their low intrinsic emission quantum yield. They also reside in various organelles including the cell membrane, the nucleus and most probably mitochondria. Their internalization depends on the porphyrin substituents as well as the cell line while their localization depends mainly on whether the cells are alive or fixed. In the latter case, this difference might be explained by the paraformaldehyde fixation which allowed the nuclear penetration and DNA binding of the compounds. Indeed, the nuclear pores situated at the nuclear envelope no longer appear to regulate the transport into the nucleus when the cells are fixed. Thus, it underlines the importance of live cell imaging to observe the real localization of the compounds.

Dark toxicity and phototoxicity

The toxicity of the hybrids was evaluated through a MTT assay (Table 3) which revealed no dark cytotoxicity for all compounds. Despite low singlet oxygen production quantum yields, illumination by a 5 J/cm² light dose allowed the measurement of IC_{50} values at the low micromolar level for monosubstituted hybrids **P_{TEG}TP** and **P_{Man}TP** and submicromolar for the disubstituted compound **$P_{TEG}(TP)_2$**. This difference is consistent with the slightly higher singlet oxygen quantum yield of **$P_{TEG}(TP)_2$** compared to monosubstituted hybrids. This could also indicate the generation of other ROS than singlet oxygen such as hydroxyl radical or superoxide anion. Further investigations are in progress to investigate this hypothesis. The mitochondrial localization is also probably responsible for these high phototoxicity efficiencies as mitochondria are the power house of the cell and disruption of mitochondrial functions via an enhanced ROS production leads to cell apoptosis.

	Dark toxicity IC_{50} (µM)		Photocytotoxicity IC_{50} (µM)	
Compound	Y79	HT-29	Y79	HT-29
P_{TEG}TP	> 7.50	> 7.50	5.68	3.34
P_{Man}TP	> 7.50	> 7.50	6.10	6.98
$P_{TEG}(TP)_2$	> 7.50	> 7.50	0.21	1.19

Table 3. Dark toxicity and phototoxicity (with light illumination; 5 J/cm^2 and excitation between 400 nm and 800 nm) of compound **P_{TEG}TP, P_{Man}TP** and **$P_{TEG}(TP)_2$** on Y79 and HT-29 cell lines.

The addition of mannosyl groups on the monosubstituted compounds barely impacted on their efficacy on either Y79 or HT-29 cells indicating no targeting effect. Meanwhile, Y79 cells showed increased susceptibility to compound **$P_{TEG}(TP)_2$** compared to HT-29 which could be linked to better cell internalization of the PS inside this cell line.

Two-photon imaging and phototoxicity

In order to verify the two-photon absorption ability of the compounds, a Leica confocal SP5 microscope coupled with Ti:Saphire femtosecond pulsed laser was used for two-photon excitation Two-photon imaging and two-photon photocytoxicity were performed on live cells using a 850nm excitation wavelength. The emission was recorded between 521 and 705 nm. 2PA excited fluorescence cell imaging of HT-29 and Y79 live cells revealed a cytoplasmic localization of the compound **$P_{TEG}(TP)_2$** without nuclear staining (Figure 8) in accordance with linear fluorescence imaging. The two others compounds **P_{TEG}TP** and **P_{Man}TP** were also detected within the two cell lines (Figures S15 and S16 respectively) thereby confirming that these compounds can be efficiently 2PA excited in live cells.

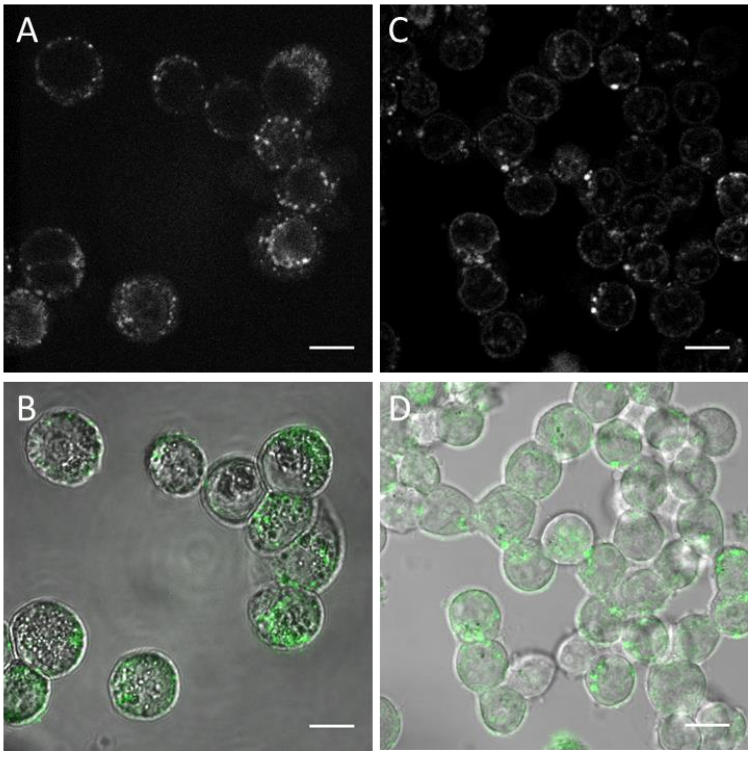

Figure 8: 2PA excited fluorescence cell imaging of HT-29 (A, B) and Y79 (C, D) live cells with $\mathbf{P_{TEG}(TP)_2}$. Overlay with brightfield (B, D). Scale bar 10 µm.

Finally, we assessed the two-photon cytotoxicity of the compounds by exposing cells in a defined area to the two-photon laser microscope as illustrated on Y79 cells with compound $\mathbf{P_{TEG}(TP)_2}$ (Figure 9). Similar results were obtained for HT-29 cells (Figure S17). The others compounds $\mathbf{P_{TEG}TP}$, $\mathbf{P_{Man}TP}$ were also tested in the two cell lines (Figures S18 and S19 respectively). Treated cells showed cellular damages after 1 minute irradiation while non-treated cells submitted to the same light dose showed no cell death. These results demonstrate the potential of this hybrid design as 2PA-PS for PDT applications.

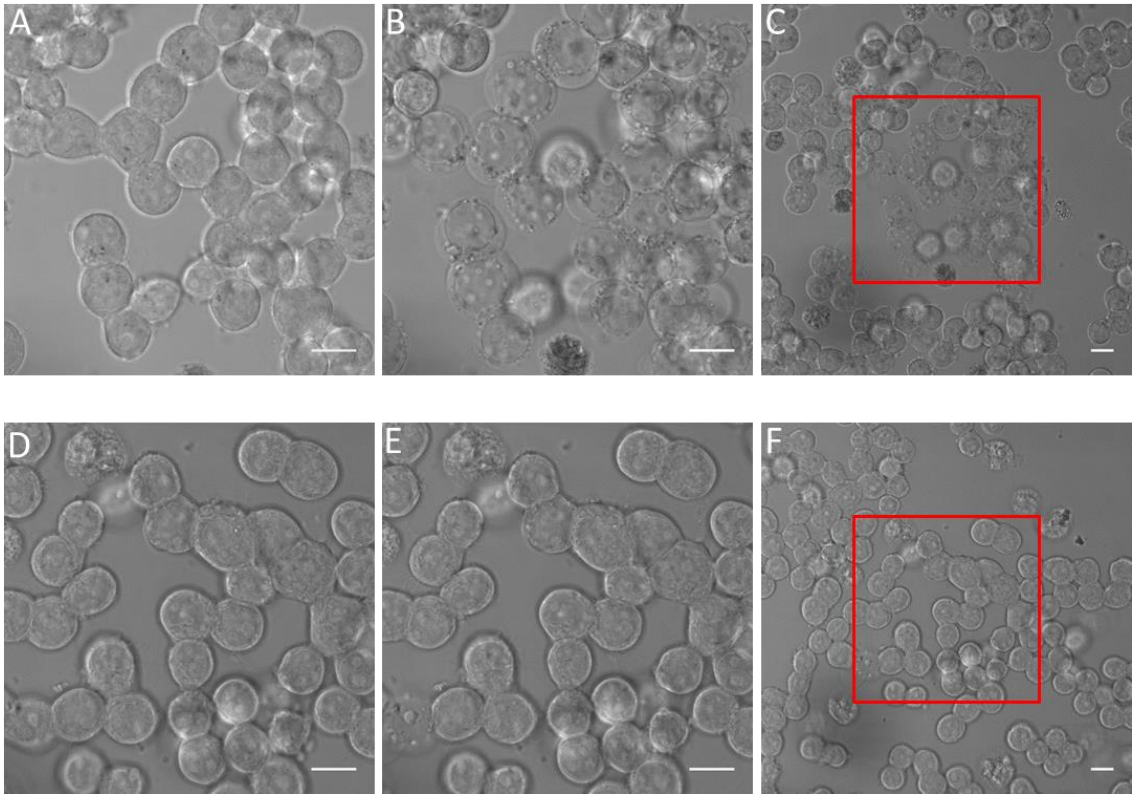

Figure 9: 2PA PDT cell imaging of Y79 live cells with (A, B, C) and without (D, E, F) $\mathbf{P_{TEG}(TP)_2}$. Before (A, D) and after scanning at 80 MHz during 1 min with Ti:Saphire laser at 850 nm (B, C, E, F). Scale bar 10 µm.

Conclusion

The cationic hybrids, compared to their neutral counterparts, display considerably improved physicochemical properties of interest for cellular application in particular enhanced water solubility and cellular internalization. Immobilization of the dyes in viscous environment led to restoration of fluorescence emission to levels comparable to that of their neutral analogs, both in terms of emission

wavelength and spectra profile. This result confirms the existence of energy transfer phenomenon between the TP and the porphyrin moieties. In contrast, the addition of duplex DNA gave rise to emission band between 520 and 620 nm.

Cellular imaging revealed that the hybrids localize partly in DNA-containing organelles, more precisely in the nucleus in fixed cells and in the mitochondria in live cells. Mitochondria are known to be highly sensitive to oxidative stress and their targeting can explain the hybrids efficacy in spite of their low singlet oxygen production.

The cationic hybrids display very promising one and two-photon photosensitizing properties against two different cancer cell lines including retinoblastoma. In contrast with our previous results, the addition of three mannosyl groups failed to guarantee specific targeting of retinoblastoma cells as phototoxicities were similar for compounds bearing one TP moiety with or without mannosyl groups. The greater photocytotoxicity was achieved for $\mathbf{P_{TEG}(TP)_2}$ which possesses two cationic TP moieties. The cellular ROS production of this promising 2PA-PS is currently under investigation.

EXPERIMENTAL SECTION

Materials and methods. All solvents used were reagent grade. Starting materials were purchased from Aldrich or Alfa Aesar and used without further purification. The following reagents have been abbreviated: dimethylformamide (DMF), dimethylsulfoxide (DMSO), 2,3-dichloro-5,6-dicyano-1,4-benzoquinone (DDQ), fetal calf serum (FCS), 3-(4,5-dimethylthiazol-2-yl)-2,5-diphenyltetrazolium bromide (MTT, Sigma, Saint-Quentin Fallavier, France), phosphate buffer saline (PBS), and Dulbecco's modified Eagle's medium (DMEM). 2-[2-(2-methoxyethoy)ethoxy]ethanol tosylate (CAS [77544-60-6]) was used without further purification. Dry MeOH was kept over 3 Å sieves, and dichloromethane was distilled from calcium hydride and kept over 4 Å sieves. DMF was distilled under slow argon flow and kept over 4 Å sieves. Column chromatography was performed with the indicated solvents using E. Merck silica gel 60 (particle size 0.035-0.070 mm). Macherey–Nagel precoated plates (SIL G-200, 2 mm) were used for preparative thin-layer chromatography. Yields refer to chromatographically and spectroscopically pure compounds. ^{1}H and ^{13}C NMR spectra were recorded with a Bruker AC-300 spectrometer (300 MHz) at ambient temperature using an internal deuterium lock. Chemical shift values are given in parts per million (ppm) relative to tetramethylsilane (TMS). Acidic impurities in $CDCl_3$ were removed by treatment with anhydrous K_2CO_3. Quantitative UV-visible spectra were recorded with a Agilent Cary Series UV-vis Spectrophotometer. Fluorescence spectra were recorded

using a Agilent Cary Eclipse fluorimeter. Measurements were performed at room temperature with solutions of OD < 0.1 to avoid re-absorption of the emitted light, and data were corrected with a blank and from the variations of the detector with the emitted wavelength. Fluorescence quantum yield were measured according to Crosby comparative method with Coumarin 153 in ethanol (Φ_F = 0.54) as reference.

The synthesis of precursors **1a**, **1b** has previously been reported by our team. Dipyrromethane was produced following existing literature.

5,15-dibromo-10,20-di({4-[2-(2-methoxyethoxy)-ethoxy]-ethoxy}-phenyl)-porphyrin zinc (II) 3. Zinc porphyrin **2** (CAS 571187-36-5) (0.40 g, 0.47 mmol, 1 eq.) was dissolved in $CHCl_3$/pyridine (40.3 mL, 99:1 v/v) . N-bromo-succinimide (0.18 g, 1.01 mmol, 2.1 eq.) was added as a solution in $CHCl_3$/pyridine (20.2mL, 99:1 v/v). The solution was stirred for 15 min at room temperature, then the reaction was quenched with acetone (1 mL) and concentrated. The crude product was washed with H_2O and filtered to give the product **3** as a red powder (0.44 g, 93 % yield). $C_{46}H_{46}Br_2N_4O_8Zn$, MW = 1008,07 g.mol^{-1}. UV-vis in CH_2Cl_2: λ_{max} nm (ε mM^{-1}.cm^{-1}): 432 (228.8), 569 (10.0), 610 (7.6). ^{1}H NMR ($CDCl_3$, 300 MHz) δ (ppm): 9.71 (d, *J* = 4.6 Hz, 4H), 8.94 (d, *J* = 4.6 Hz, 4H), 8.07 (d, *J* = 8.4 Hz, 4H), 7.05 (d, *J* = 8.4 Hz, 4H), 4.46-4.38 (m, 4H), 4.09-4.02 (m, 4H), 3.90-3.82 (m, 4H), 3.80-3.75 (m, 4H), 3.64-3.56 (m, 4H), 3.22-3.42 (s, m, 4H), 2.89-2.79 (s, 6H). ^{13}C NMR ($CDCl_3$, 75.3 MHz) δ (ppm): 158.7, 151.1, 149.1, 135.3, 135.2, 132.1, 131.5, 120.6, 120.1, 112.5, 100.0, 71.1-66.0, 58.5. MS (MALDI-TOF): $[M]^+$ ($C_{46}H_{46}Br_2N_4O_8Zn$) m/z calc. = 1004.10, found = 1004.11.

5,15-di(trimethylsilyl)ethynyl-10,20-di({4-[2-(2-methoxyethoxy)-ethoxy]-ethoxy}-phenyl)-porphyrin zinc (II) 4. The brominated porphyrin **3** (0.85 g, 0.86 mmol, 1 eq.), bis(triphenylphosphine)-palladium(II) dichloride ($[Pd(PPh_3)]_2Cl_2$, 60.2 mg, 86 µmol, 10 mol%) and copper(I) iodide (16.3 mg, 86 µmol, 10 mol%) were put necked flask. A cycle of vide-Ar was done, then THF (20 mL) and triethylamine (2.5 mL) were added. The solution was degassed by purging with argon for 10 min, then cooled in liquid nitrogen, and trimethylsilylacetylene (1.01 g, 0.70 mmol, 0.8 eq.) was added. After stirring 1h, the reaction mixture was warmed to room temperature and stirred for 16 h and then quenched with H_2O (3 mL). The mixture was extracted by CH_2Cl_2 and the organic layer was washed with H_2O (3×30 mL) and brine (30 mL). The organic layer was dried over $MgSO_4$, filtered and purified by column chromatography over silica gel (CH_2Cl_2/EtOH 95:5, v/v) to give the expected product as a dark green powder (0.71 g, 84% yield). $C_{56}H_{64}N_4O_8Si_2Zn$, MW = 1042.68 g.mol^{-1}. UV-vis in CH_2Cl_2: λ_{max} nm (ε mM^{-1}.cm^{-1}): 439 (218.3), 451 (150.4), 588 (7.7), 640 (24.6). ^{1}H NMR ($CDCl_3$, 300 MHz) δ (ppm): 9.71 (d, *J* = 4.6 Hz, 4H), 8.94 (d, *J* = 4.6 Hz, , 4H), 8.08 (d, *J* = 8.5 Hz, , 4H), 7.24 (d, *J* = 8.5 Hz, 4H), 4.32-

4.10 (m, 4H), 4.04-3.73 (m, 4H), 3.69-3.59 (m, 4H), 3.55-3.45 (m, 4H), 3.46-3.30 (m, 4H), 3.30-3.22 (m, 4H), 3.13 (s, 6H), 0.64 (s, 18H). ^{13}C NMR ($CDCl_3$, 75.3 MHz) δ (ppm): 157.0, 151.7, 150.1, 135.0, 134.5, 132.2, 130.6, 121.8, 112.2, 107.6, 100.9, 100.4, 70.8-66.9, 58.1, 0.5. MS (MALDI-TOF): $[M]^+$ ($C_{56}H_{64}N_4O_8Si_2Zn$) m/z calc. = 1040.36, found = 1040.36.

5,15-di-(N,N-bis-(4-formylphenyl)-4'-anilinoethynyl)-10,20-di({4-[2-(2-methoxyethoxy)-ethoxy]-etho-xy}-phenyl)-porphyrin zinc (II) 5. The porphyrin **4** (0.20 g, 0.20 mmol, 1 eq.) was dissolved in THF/ CH_2Cl_2 (24 mL, 83:17 v/v), then tetra-*n*-butylammonium fluoride (0.12 g, 0.53 mmol, 2.7 eq.) was added. The solution was stirred for 30 min. Then, $CaCl_2$ was added and the mixture was stirred for further 5 min and filtered. The filtrate was washed with H_2O (3×60 mL), dried over $MgSO_4$ and filtered. The intermediary product was introduced in a dry two necked flask. Tri(diben-zylideneacetone)-dipalladium ($[Pd_2(dba)_3]$, 28.7 mg, 0.12 mmol, 0.6 eq.), 4,4'-diformyl-4''-iodotriphenylamine (324.7 mg, 0.76 mmol, 3.8 eq.) and triphenylarsine (187.4 mg, 0.61 mmol, 3 eq.) were added. The system was degassed by purging with argon for 20 min, and then THF/triethylamine (20 mL, 1:1 v/v) were added. The mixture was stirred for 20 h at room temperature. After evaporation, the solid was dissolved in CH_2Cl_2 (25 mL) and washed with H_2O (3×30 mL). The organic layer was dried over $MgSO_4$, filtered and purified by column chromatography over silica gel (CH_2Cl_2:EtOH from 99:1 to 95:5, v/v) to afford product **5** as a green powder (0.13 g, yield 46%). $C_{90}H_{74}N_6O_{12}Zn$, M = 1496,96 g.mol^{-1}. UV-vis in CH_2Cl_2: λ_{max} nm (ε mM^{-1}.cm^{-1}): 375 (37.6), 460 (245.8), 669 (48.5). ^{1}H NMR ($CDCl_3$, 300 MHz) δ (ppm): 9.69 (d, *J* = 4.6 Hz, 4H), 9.63 (s, 4H), 8.92 (d, *J* = 4.6 Hz, 4H), 8.02 (d, *J* = 8.3 Hz, 4H), 7.86 (d, *J* = 8.4 Hz, 4H), 7.52 (d, *J* = 8.5 Hz, 8H), 7.07 (d, *J* = 8.3 Hz, 4H), 7,00 (d, *J* = 8.4 Hz, 4H), 6.89 (d, *J* = 8.5 Hz, 8H), 3.85-3.75 (m, 4H), 3.45-3.35 (m, 4H), 3.25-3.17 (m, 4H), 3.12-3.04 (m, 4H), 3.02-2.96 (m, 4H), 2.96-2.90 (m, 4H), 2.80 (s, 6H). ^{13}C NMR ($CDCl_3$, 75.3 MHz) δ (ppm): 190.5, 158.4, 151.9, 151.3, 150.5, 145.3, 135.5, 134.9, 133.1, 132.9, 131.5, 131.3, 130.8, 126.4, 123.1, 122.8, 121.3, 112.8, 101.1, 96.0, 94.1, 71.3, 70.2, 69.9, 69.8, 69.3, 67.2, 58.5. HRMS (MALDI-TOF): $[M+Na]^+$ ($C_{90}H_{74}N_6O_{12}ZnNa$) m/z calc. = 1517.4554, found = 1517.4535.

5,15-di-(N,N-bis-(4'-(E)-2-(pyridine-4-yl)-vinyl)-phenyl)-4'-anilinoethynyl)-10,20-di({4-[2-(2-metho-xyethoxy)-ethoxy]-ethoxy}-phenyl)-porphyrin zinc (II) 6. To a suspension of sodium hydride (15.1 mg, 0.63 mmol, 9.4 eq.) in THF (2 mL) was added diethyl(4-pyridinyl)methyl phosphonate (128.4 mg, 0.56 mmol, 8.4 eq.), then a solution of porphyrin **5** (100.5 mg, 0.067 mmol, 1 eq.) in THF (2 mL) was added dropwise . The mixture was stirred for 24 h at room temperature. After concentration, the crude residue was dissolved in CH_2Cl_2 (5 mL) and washed with $NaHCO_3$ sat. (10 mL) and H_2O (3×10 mL). The organic layer was dried over $MgSO_4$, filtered, concentrated and purified by column chromatography over silica gel (CH_2Cl_2/EtOH from 99:1 to 95:5, v/v) to give the product **6** as a purple

powder (70 mg, 58%). $C_{114}H_{94}N_{10}O_8Zn$, M = 1797,41 g:mol^{-1}. UV-vis in CH_2Cl_2: λ_{max} nm (ε mm^{-1}.cm^{-1}): 470 (89.5), 685 (33.7). ^{1}H NMR ($CDCl_3$, 300 MHz) δ (ppm): 9.65 (d, *J* = 4.5 Hz, 4H), 8.83 (d, *J* = 4.6 Hz, 4H), 8.04 (d, *J* = 8.5 Hz, 4H), 7.87 (d, *J* = 8.4 Hz, 4H), 7.30 (d, *J* = 8.5 Hz, 8H), 7.27-7.22 (m, 4H), 7,19 (d, *J* = 8.4 Hz, 4H), 7.06 (d, *J* = 8.5 Hz, 8H), 6.99 (d, *J* = 16.1 Hz, 4H), 6.90-6.81 (m, 8H), 6.63 (d, *J* = 16.1 Hz, 4H), 4.48-4.34 (m, 4H), 4.09-4.01 (m, 4H), 3.90-3.82 (m, 4H), 3.81-3.76 (m, 4H), 3.75-3.70 (m, 4H), 3.64-3.57 (m, 4H), 3.41 (s, 6H). ^{13}C NMR ($CDCl_3$, 75.3 MHz) δ (ppm): 158.5, 151.9, 150.4, 148.5, 147.3, 146.8, 144.9, 135.6, 135.4, 132.8-132.6, 131.2, 128.3, 124.2-124.2, 122.5, 120.4, 119.3, 112.7, 100.1, 96.3, 93.7, 72.1, 71.0, 70.8, 70.7, 70.0, 67.8, 59.2. MS (MALDI-TOF): $[M]^+$ ($C_{114}H_{94}N_{10}O_8Zn$) m/z calc. = 1794.65 m/z found = 1794.65.

General methylation procedure. The unmethylated hybrids were dissolved in anhydrous DMF. Then 70 eq. of methyl iodide (MeI) were added and the mixture was stirred at room temperature in the dark for 18 h. The mixture was concentrated to dryness affording the title compounds. No further purification was required.

20-{N,N-bis-[4'-(2'-(N-methylpyridin-4-ylium)-vinyl)-phenyl]-4-anilino-ethynyl}-5,10,15-tris(4-{[((methoxy)-ethoxy)-ethoxy]-ethoxy}-phenyl)-porphyrinato Zinc (II) diiodide P_{TEG}TP. According to the procedure used for the preparation of **P_{TEG}TP** from compound **1a** (100 mg, 71 µmol, 1 eq.) was combined with MeI (309 µL, 4,97 mmol, 70 eq.) in 3.5 mL DMF. The expected product was isolated as a brown solid (118 mg, 100 %). $C_{95}H_{95}I_2N_7O_{12}Zn$, M = 1846.44 g.mol^{-1}. UV-vis in CH_2Cl_2: λ_{max} nm (ε mM^{-1}.cm^{-1}): 448 (128.6), 638 (24.0). ^{1}H NMR (DMF-d_7, 300 MHz) δ (ppm): 9.86 (d, *J* = 4.6 Hz, 2H), 8.94 (d, *J* = 4.6 Hz, 2H), 8.91 (d, *J* = 6.4 Hz, 4H), 8.84 (s, 4H), 8.29 (d, *J* = 6.4 Hz, 4H), 8.22-8.10 (m, 10H), 7.82 (d, *J* = 8.4 Hz, 4H), 7.52 (d, *J* = 16.2 Hz, 2H), 7.44-7.28 (m, 8H), 7.19 (d, *J* = 8.3 Hz, 4H), 4.38 (s, 6H), 4.34-4.27 (m, 6H), 3.94-3.88 (m, 6H), 3.74-3.67 (m, 6H), 3.66-3.56 (m, 12H), 3.52-3.47 (m, 6H,), 3.29 (s, 9H). ^{13}C–NMR (DMF-d_7, 75.3 MHz) δ (ppm): 158.9, 153.5, 152.2, 150.9, 150.4, 150.1, 148.63 146.6, 145.3, 140.7, 135.8, 135.4, 135.3, 133.3, 132.9, 132.2, 131.8, 131.1, 130.7, 130.3, 125.6, 124.4, 123.7, 122.9, 122.2, 121.9, 119.9, 113.0, 99.0, 96.1, 93.9, 72.0, 70.8, 70.6, 70.4, 69.8, 68.1, 58.3. HRMS (MALDI-TOF): $[M-2I]^+$ ($C_{95}H_{95}N_7O_{12}Zn$) m/z calc. = 1589.63192, found= 1589.63486.

20-{N,N-bis-[4'-(2'-(N-methylpyridin-4-ylium)-vinyl)-phenyl]-4-anilino-ethynyl}-5,10,15-tris{4-O-([2-O-(α-D-mannosyloxy)-ethoxy]-ethoxy)-phenyl}-porphyrin Zinc (II) diiodide P_{Man}TP . According to the general procedure **P_{Man}TP** was prepared from compound **1b** (30 mg, 16 µmol, 1 eq.) was combined with MeI (100 µL, 1,12 mmol, 70 eq.) in 1 mL dry DMF. The expected product was isolated as a brown solid (34 mg, 98 %). $C_{104}H_{107}I_2N_7O_{24}Zn$, M = 2158.47 g.mol^{-1}. UV-vis in DMF: λ_{max} nm (ε mM^{-1}.cm^{-1}): 450 (130.2), 638 (24.1). ^{1}H NMR (DMF-d_7, 300 MHz) δ (ppm): 9.83 (d, *J* = 4.7 Hz, 2H), 9.22 (d, *J* = 6.0

Hz, 2H), 9.01 (d, *J* = 6.3 Hz, 4H), 8.95 (d, *J* = 4.7 Hz, 2H), 8.35 (d, *J* = 6.3 Hz, 4H), 8.30-8.08 (m, 10H), 7.88 (d, *J* = 8.3 Hz, 4H), 7.60 (d, *J* = 16.2 Hz, 2H), 7.41 (d, *J* = 7.8 Hz, 6H), 7.31 (d, *J* = 8.2 Hz, 4H), 4.92-4.80 (m, 9H), 4.58 (s, 6H), 4.54-4.39 (m, 9H), 4.05-3.97 (m, 9H), 3.94-3.78 (m, 9H), 3.74 – 3.54 (m, 9H). ^{13}C–NMR (DMF-d_7, 75.3 MHz) δ (ppm):170.7, 170.3,159.0, 153.7, 152.2, 153.0, 150.4 150.1, 148.8, 146.3, 145.6, 145.5, 140.8, 135.9, 135.4, 131.2, 130.3, 128.3, 125.7, 124.5, 123.8, 121.9, 113.1, 101.1, 98.9, 96.0, 74.5, 73.4, 72.2, 71.3, 70.6, 69.9, 68.2, 66.6, 62.4, 61.4, 48.4, 47.2. HRMS (MALDI-TOF): $[M-2I]^+$ ($C_{104}H_{107}N_7O_{24}Zn$) m/z calc. = 1901.66480, found = 1901.65901.

10,20-bis-{N,N-bis-[4'-(2'-(N-methylpyridin-4-ylium)-vinyl)-phenyl]-4-anilino-ethynyl}-5,15-bis(4-{[((methoxy)-ethoxy)-ethoxy]-ethoxy}phenyl)-porphyrin Zinc (II) tetraiodide $P_{TEG}(TP)_2$. According to the general procedure **$P_{TEG}(TP)_2$** was synthesized from compound **6** (30 mg, 17 µmol. 1 eq.) was combined with MeI (74 µL, 1.19 mmol, 70 eq.) in 1.5 mL dry DMF. The expected product was isolated as a brown solid (38 mg, 94 %). $C_{118}H_{106}I_4N_{10}O_8Zn$, M = 2365.16 g.mol^{-1}. UV-vis in CH_2Cl_2: λ_{max} nm (ε mM^{-1}.cm^{-1}): 474 (76.2), 695 (23.5). ^{1}H NMR (DMSO-d_6, 300 MHz) δ (ppm): 9.70 (d, *J* = 4.6 Hz, 4H,), 8.86-8.78 (m, 12H), 8.19 (d, *J* = 6.5 Hz, 8H), 8.15-7.96 (m, 12H), 7.79 (d, *J* = 8.5 Hz, 8H), 7.50-7.32 (m, , 12H), 7.27 (d, *J* = 8.5 Hz, 8H), 4.46-436 (m, 4H), 4.24 (s, 12H), 3.98-3.91 (m, 4H), 3.76-3.70 (m, 4H), 3.68-3.58 (m, 8H), 3.54-3.48 (m, 4H), 3.29 (s, 6H). HRMS (MALDI-TOF): $[M-4I]^+$ ($C_{114}H_{106}N_{10}O_8Zn$) m/z calc. = 1854.7487, found = 1854.7300.

Comparative singlet oxygen production. An aerated solution of 1,3-diphenylisobenzofuran (DPBF) (5 x 10^{-5} M) and photosensitizer (10^{-6} M) in recently distilled DMF (50 mL) was irradiated with white light (home-made source) at 25 °C for 5 min. Aliquots (3 mL) were removed from the solution at 1 min intervals and stored in inactinic vials. Reaction of DPBF with $^1O_2$ was monitored by the decreasing intensity of the absorption band at 411 nm over time. Irradiation of aerated DPBF solution without photosensitizer gave no significant reduction in intensity of the 411 nm absorption band.

Studies of interactions with DNA. The variation of the fluorescence signal of a fluorophore solution of fixed concentration (1 µM) was monitored upon addition of increasing quantities of DrewAT, a 14 base pair oligonucleotide (sequence: 5'-CGCGAAATTTCGCG). A quick UV titration of the fluorophore (10 µM) by the oligonucleotide was first performed to determine the isobestic point when there is one. The excitation wavelength was then chosen so as to minimize the variation of the absorbance upon addition of DNA. The fluorimetric titration curves were obtained by plotting F/F_0 versus the concentration of oligonucleotide, where F is the integrated fluorescence intensity of the

oligonucleotide-dye complex and F_0 the initial fluorescence of the free dye between 500 and 620 nm to remove the porphyrinic contribution to the emission.

General procedures for *in vitro* experiments

Cell culture conditions. The Y79 (Human retinoblastoma cells, ATCC® HTB-18™) and HT-29 (Human colorectal adenocarcinoma cells, ATCC® HTB-38™) cell lines were obtained from the American Type Culture Collection (ATCC®, Manassas, VA, USA,)). Y79 cells were cultured in suspension in Dulbecco's modified Eagle's medium (DMEM, Life Technologies, Saint-Aubin, France) GlutaMAX™ supplemented with 20 % fetal calf serum (FCS, South America origin, BioWhittaker® Lonza, Verviers, Belgium) and 1% Penicillin/Streptomycin (Life Technologies) in humidified atmosphere under 5% CO_2 in air at 37 °C. Adherent HT-29 cells were grown to confluence in DMEM Glutamax™ supplemented with 10 % FCS and 1 % Penicillin/Streptomycin in humidified atmosphere under 5 % CO_2 in air at 37 °C. Cells were subcultured by dispersal subcultured twice a week by dispersal with TrypLE™ Express Enzyme (Life Technologies).

Photocytotoxicity assay. For Y79 cells and HT-29 cells, $1.5.10^5$ and $0.5.10^5$ cells/well in 1 mL respectively, were seeded into 24-microwell plates with the appropriate culture medium. After 3 h of incubation at 37 °C for Y79 and 24 h for HT-29, tested compounds, in dimethyl sulfoxide (DMSO, Sigma-Aldrich, Saint-Quentin Fallavier, France) stock solution, were added in the dark at a final concentration ranging from 0.15 to 7.5 μM. Control cells received 7.5 μL of DMSO (0.75 %) free of dye. After 24 h of incubation with PS at 37 °C in the dark, medium was removed and fresh medium free of dye was added for adherent HT-29 cells whereas Y79 cells cultured in suspension were left with the compounds. Then, illumination was performed (5 J/cm^2) through the bottom of the 24-microwell plates using a 'light box' made of six Phillips TL 13W tubes (mono photon emission wavelengths from 400 to 800 nm), leading to a final fluence of 3 mW/cm^2. Plates were left to incubate in the dark for 3 days before evaluation of the cell viability by determination of mitochondrial activity using the 3-[4,5-dimethylthiazol-2-yl]-2,5-diphenyl tetrazolium bromide assay (MTT, Sigma-Aldrich). At the time of counting, 50 μL of a MTT (5 mg/mL) solution was added to each well. After 30 min of incubation and removal of the medium, formazan crystals were taken up with 600 μL of DMSO and absorbance at 562 nm was measured with a Fluostar™ microplate reader (BMG LABTECH, Champigny sur Marne, France). Cellular viability was expressed as percentage of untreated controls. IC_{50} values corresponding to the concentration of drug leading to 50 % survival were interpolated from the dose response curves and are expressed in μM. Each concentration in the same experiment was carried out in duplicate and the experiment was repeated at least three times.

One and two-photon cellular imaging. For fixed cells, 5.10^5 HT-29 cells were seeded onto glass

coverslips (diameter 22 mm, thickness 0.17 mm) in six-well plates with DMEM without phenol red supplemented with 10 % FCS and antibiotics. After 24 h, the studied compound was added to a final concentration of 5 μM in culture medium. Control cells were incubated with 0.5 % DMSO in culture medium. After 24 h of incubation in the dark, cells were fixed with 3 % paraformaldehyde (Electron Microscopy Sciences, Hatfield, PA, USA) in PBS (20 min). Cells were then washed 3 times with PBS (10 min each), rinsed twice with 0.1 % (w/v) NH_4Cl in PBS (10 min each), and re-washed 3 times with PBS (5 min each). After washing, coverslips were mounted on slide with ProLong® Gold antifade reagent (Life Technologies, Saint Aubin, France). In the same way as described above, 1.10^6 Y79 cells were seeded onto poly-L-lysine coated (Sigma-Aldrich) glass coverslips and treated.

For live cells, 5.10^5 HT-29 cells per well were seeded onto two-well Nunc® Lab-Tek® II Chambered Cover glass (Thermoscientific, Langenselbold, Germany) in culture medium without phenol red. After 24 h of incubation the compound was added to a final concentration of 5 μM in culture medium without phenol red. Control cells were incubated with 0.5 % DMSO in culture medium. In the same way as described above, 1.10^6 Y79 cells were seed onto poly-L-lysine coated two-well Nunc® Lab-Tek® II Chambered Cover glass. After incubation, the medium containing the dye was replaced with fresh medium without phenol red. Images of fields were acquired on a Leica confocal SP5 system equipped with a Plan APO CS 63.0x OIL UV (NA 1.4) objective and coupled with an argon gas laser (458 nm) and helium neon gas laser (633 nm) for one-photon excitation and a Ti:Saphire laser delivering pulses in the 100-200 fs range at an 80 MHz repetition rate with a tenability ranging from 705 to 980 nm for two-photon excitation. The images were visualized and processed using the Image J software (Rasband W.S., U. S. National Institutes of Health, Bethesda, Maryland, USA).

AUTHOR INFORMATION

Corresponding Authors

*E-mail: florence.mahuteau@curie.fr Tel: +33 1 69 86 71 59

*E-mail: fabien.hammerer@gmail.com Tel:+1 (514) 398 6229

ACKNOWLEDGMENTS

The authors acknowledge CNRS, the 'Programme Incitatif et Coopératif Rétinoblastome et Transcriptome' of Institut Curie, and the nonprofit French organization "Rétinostop" (http://www.retinostop.fr) for their financial support. F.H. thanks Université Paris-Sud and ENS Cachan for Ph.D. funding, S.C. thanks "la région Ile de France", subsidy PICRI 2012, for Ph.D. funding. This work has benefited from the facilities of the Small Molecule Mass Spectrometry platform of IMAGIF (Centre de Recherche de Gif - www.imagif.cnrs.fr). We are also very grateful to Marine

Scoazec and Marie-Noelle Soler from the imaging plateform PICT-IBISA@ORSAY (Institut Curie, Orsay, France) for technical assistance in the use of the Leica confocal SP5 system. We acknowledge Dr. Céline Frochot and Dr. Philippe Arnoux from LGRP-UMR 7274 at ENSIC Nancy for the singlet oxygen measurements.

ASSOCIATED CONTENT

Supporting Information.

REFERENCES

(1) Kessel, D. (2015) More Adventures in Photodynamic Therapy. *International journal of molecular sciences 16*, 15188-93.

(2) van Straten, D., Mashayekhi, V., de Bruijn, H. S., Oliveira, S., and Robinson, D. J. (2017) Oncologic Photodynamic Therapy: Basic Principles, Current Clinical Status and Future Directions. *Cancers 9*.

(3) Agostinis, P., Berg, K., Cengel, K. A., Foster, T. H., Girotti, A. W., Gollnick, S. O., Hahn, S. M., Hamblin, M. R., Juzeniene, A., Kessel, D., Korbelik, M., Moan, J., Mroz, P., Nowis, D., Piette, J., Wilson, B. C., and Golab, J. (2011) Photodynamic therapy of cancer: an update. *CA: a cancer journal for clinicians 61*, 250-81.

(4) Celli, J. P., Spring, B. Q., Rizvi, I., Evans, C. L., Samkoe, K. S., Verma, S., Pogue, B. W., and Hasan, T. (2010) Imaging and photodynamic therapy: mechanisms, monitoring, and optimization. *Chemical reviews 110*, 2795-838.

(5) Dolmans, D. E., Fukumura, D., and Jain, R. K. (2003) Photodynamic therapy for cancer. *Nature reviews. Cancer 3*, 380-7.

(6) Collins, H. A., Khurana, M., Moriyama, E. H., Mariampillai, A., Dahlstedt, E., Balaz, M., Kuimova, M. K., Drobizhev, M., YangVictor, X. D., Phillips, D., Rebane, A., Wilson, B. C., and Anderson, H. L. (2008) Blood-vessel closure using photosensitizers engineered for two-photon excitation. *Nat Photon 2*, 420-424.

(7) Hu, W., He, T., Jiang, R., Yin, J., Li, L., Lu, X., Zhao, H., Zhang, L., Huang, L., Sun, H., Huang, W., and Fan, Q. (2017) Inner salt-shaped small molecular photosensitizer with extremely

enhanced two-photon absorption for mitochondrial-targeted photodynamic therapy. *Chemical communications 53*, 1680-1683.

(8) Lan, M., Zhao, S., Xie, Y., Zhao, J., Guo, L., Niu, G., Li, Y., Sun, H., Zhang, H., Liu, W., Zhang, J., Wang, P., and Zhang, W. (2017) Water-Soluble Polythiophene for Two-Photon Excitation Fluorescence Imaging and Photodynamic Therapy of Cancer. *ACS applied materials & interfaces 9*, 14590-14595.

(9) Oheim, M., Michael, D. J., Geisbauer, M., Madsen, D., and Chow, R. H. (2006) Principles of two-photon excitation fluorescence microscopy and other nonlinear imaging approaches. *Advanced drug delivery reviews 58*, 788-808.

(10) Wang, B. G., Konig, K., and Halbhuber, K. J. (2010) Two-photon microscopy of deep intravital tissues and its merits in clinical research. *Journal of microscopy 238*, 1-20.

(11) Starkey, J. R., Rebane, A. K., Drobizhev, M. A., Meng, F., Gong, A., Elliott, A., McInnerney, K., and Spangler, C. W. (2008) New two-photon activated photodynamic therapy sensitizers induce xenograft tumor regressions after near-IR laser treatment through the body of the host mouse. *Clinical cancer research : an official journal of the American Association for Cancer Research 14*, 6564-73.

(12) Hammerer, F., Garcia, G., Chen, S., Poyer, F., Achelle, S., Fiorini-Debuisschert, C., Teulade-Fichou, M. P., and Maillard, P. (2014) Synthesis and characterization of glycoconjugated porphyrin triphenylamine hybrids for targeted two-photon photodynamic therapy. *The Journal of organic chemistry 79*, 1406-17.

(13) Laville, I., Pigaglio, S., Blais, J. C., Doz, F., Loock, B., Maillard, P., Grierson, D. S., and Blais, J. (2006) Photodynamic efficiency of diethylene glycol-linked glycoconjugated porphyrins in human retinoblastoma cells. *Journal of medicinal chemistry 49*, 2558-67.

(14) Griegel, S., Rajewsky, M. F., Ciesiolka, T., and Gabius, H. J. (1989) Endogenous sugar receptor (lectin) profiles of human retinoblastoma and retinoblast cell lines analyzed by cytological markers, affinity chromatography and neoglycoprotein-targeted photolysis. *Anticancer research 9*, 723-30.

(15) Dumat, B., Bordeau, G., Faurel-Paul, E., Mahuteau-Betzer, F., Saettel, N., Metge, G., Fiorini-Debuisschert, C., Charra, F., and Teulade-Fichou, M. P. (2013) DNA switches on the two-

photon efficiency of an ultrabright triphenylamine fluorescent probe specific of AT regions. *Journal of the American Chemical Society 135*, 12697-706.

(16) Chennoufi, R., Bougherara, H., Gagey-Eilstein, N., Dumat, B., Henry, E., Subra, F., Mahuteau-Betzer, F., Tauc, P., Teulade-Fichou, M. P., and Deprez, E. (2015) Differential behaviour of cationic triphenylamine derivatives in fixed and living cells: triggering and imaging cell death. *Chemical communications 51*, 14881-4.

(17) Rui, L., Xue, Y., Wang, Y., Gao, Y., and Zhang, W. (2017) A mitochondria-targeting supramolecular photosensitizer based on pillar[5]arene for photodynamic therapy. *Chemical communications 53*, 3126-3129.

(18) Chakrabortty, S., Agrawalla, B. K., Stumper, A., Vegi, N. M., Fischer, S., Reichardt, C., Kogler, M., Dietzek, B., Feuring-Buske, M., Buske, C., Rau, S., and Weil, T. (2017) Mitochondria Targeted Protein-Ruthenium Photosensitizer for Efficient Photodynamic Applications. *Journal of the American Chemical Society 139*, 2512-2519.

(19) Fulda, S., Galluzzi, L., and Kroemer, G. (2010) Targeting mitochondria for cancer therapy. *Nature reviews. Drug discovery 9*, 447-64.

(20) Chang, C. C., Hsieh, M. C., Lin, J. C., and Chang, T. C. (2012) Selective photodynamic therapy based on aggregation-induced emission enhancement of fluorescent organic nanoparticles. *Biomaterials 33*, 897-906.

(21) Chennoufi, R., Bougherara, H., Gagey-Eilstein, N., Dumat, B., Henry, E., Subra, F., Bury-Mone, S., Mahuteau-Betzer, F., Tauc, P., Teulade-Fichou, M. P., and Deprez, E. (2016) Mitochondria-targeted Triphenylamine Derivatives Activatable by Two-Photon Excitation for Triggering and Imaging Cell Apoptosis. *Scientific reports 6*, 21458.

TABLE OF CONTENTS GRAPHIC